Optics Letters

Cost-effective imaging of optoacoustic pressure, ultrasonic scattering, and optical diffuse reflectance with improved resolution and speed

PAVEL SUBOCHEV

Institute of Applied Physics, 46 Ulyanov Street, Nizhny Novgorod 603950, Russia (Pavel. Subochev@gmail.com)

Received 13 November 2015; revised 31 December 2015; accepted 19 January 2016; posted 20 January 2016 (Doc. ID 253895); published 29 February 2016

The idea of a method of cost-effective upgrades from an acoustic resolution photoacoustic microscope to a triple-modality imaging system is validated using phantoms. The newly developed experimental setup is based on a diode pumped solid state laser coupled to a fiber bundle with a spherically focused polyvinylidene fluoride detector integrated into the center of a ring shaped optical illuminator. Each laser pulse illuminating the sample performs two functions. While the photons absorbed by the sample provide a measurable optoacoustic (OA) signal, the photons absorbed by the detector provide the measurable diffuse reflectometry (DR) signal from the sample and the probing ultrasonic (US) pulse. At a 3 mm imaging depth, the axial resolution of the OA/US modalities is 38 μm/26 μm, while the lateral resolution of the DR/OA/US modalities is 3.5 mm/50 μm/35 μm. The maximum acquisition rate of the trimodal DR/OA/US A-scans is 2 kHz.

OCIS codes: (170.5120) Photoacoustic imaging; (170.7180) Ultrasound diagnostics; (230.5160) Photodetectors; (120.4825) Optical time domain reflectometry.

http://dx.doi.org/10.1364/OL.41.001006

Optoacoustic (OA) (or photoacoustic) methods of biomedical visualization [1] are based on the remote detection of *ultrasonic* (US) pulses generated due to the absorption of nanosecond laser pulses by heterogeneities of optical absorption. The optical absorption coefficient of the background biological tissues is usually orders of magnitude smaller than the reduced optical scattering coefficient [2], allowing deep penetration by the scattered photons [3]. At diagnostic depths greater than the transport length of the photons, the resolution of OA methods is defined by the frequency of the US detector [4]. However, since the frequency-dependent US penetration in soft tissues meets the effective optical penetration for the visible range at approximately 50 MHz [5], the methods of biomedical OA imaging are the most useful at a mesoscopic scale [6,7] corresponding to an average diagnostic depth of 3 mm.

When compared to US mesoscopy and optical *diffuse reflectometry* (DR) individually, OA methods provide higher contrast and spatial resolution. Nevertheless, the combination of OA imaging with DR and US holds much promise. The heterogeneities of optical and acoustic scattering imaged by DR [8] and US [9] modalities can provide important anatomical guidance for OA images [10].

This Letter investigates the opportunity of obtaining simultaneous OA/DR/US mesoscopic imaging in reflection-mode, using conventional OA hardware. To provide cost-effective DR/US sensing simultaneously with OA, we propose the use of photons back-scattered from the sample toward an acoustic detector, generating a measurable DR signal [11] as well as the US probing pulse [12].

The laser-ultrasound excitation of the probing US pulses by optical illumination has been used in the tomographic OA systems of other authors [13,14]. The raster-scan OA/US system reported by our group [15] suffered from relatively poor lateral resolution (200 μm for OA and 140 μm for US) as well as low acquisition speed (10 A-scans per second). The novel system being reported in this Letter demonstrates several important improvements. First, the new system is capable of an additional DR modality [16] provided by measurements of the amplitude of the probing US pulse. Second, the new system has achieved a four-fold improvement in the lateral OA/US resolution provided by a custom-made OA detector with a numerical aperture of 0.6. Third, the novel system demonstrates a two order improvement in the imaging speed, provided by a laser with a 2 kHz pulse repetition rate. Finally, it presents a new way for improving the contrast and the diagnostic depth of the OA modality through simultaneous excitation of the sample at the optical wavelengths 532 and 1064 nm (within the same laser pulse).

The experimental setup for triple-modality OA/US/DR imaging is presented in Fig. 1. The scanning OA head [Fig. 1(a)] is based on a fiber bundle (CeramOptec, Germany) containing 77 fibers of a 0.12 numerical aperture, with 70 fibers arranged at a 37° angle to the Z axis [Fig. 1(b)] and 7 fibers used for beam sampling. A custom made, spherically focused 35 MHz *polyvinylidene fluoride* (PVDF) detector [Fig. 1(c)] with a 30 MHz bandwidth, a $F = 6.8$ mm focal length, and a 0.6 numerical aperture is placed at the center of the ferrule [Fig. 1(b)] containing the output tips of the fibers. The axial geometry of the optical illumination and acoustic detection is represented in Fig. 1(d),

where $z_F = 5$ mm is a distance from the OA head, corresponding to the optical and acoustic foci. The lateral geometry of the optical illumination at different distances from the OA head is shown in Figs. 1(e)–1(g). The distance from the OA head to the sample $z_0 = 2$ mm provides a ring shaped optical illumination of the sample with a 0.2 cm^2 effective area at the sample's surface [Fig. 1(f)] and dark-field acoustic detection [7]. In case of US detection through the dark center of optical illumination, geometrical optical and acoustic foci [Fig. 1(e)] are located at $z_F - z_0 = 3$ mm depth below the surface of the sample.

The OA head is mounted on two computer-driven M-664 stages with a 25 mm travel range and 400 mm/s maximum velocity. The low-jitter input of the laser Wedge HB 532 (BrightSolutions, Italy) is triggered by the scanning stages and provides a pulse repetition rate of up to 2 kHz with a 1.4 ns pulse duration and a maximum pulse energy of 1.5 mJ distributed between two wavelengths (with 1 mJ power at 532 nm and 0.5 mJ at 1064 nm). The maximum radiant exposure at the sample surface is 7.5 mJ/cm^2, and this level is therefore always below the 20 mJ/cm^2 ANSI Z136.1 standard for laser safety. Depending on the optical properties of the sample [2], a set of optical filters placed between the laser and the fiber bundle allows a choice of 532, 1064, or both 532 and 1064 nm wavelengths to optimize the contrast and the diagnostic depth of the OA modality. However, all the phantom experiments related to this Letter utilize only the 532 nm optical wavelength and a 0.3 mJ laser pulse energy, providing only 1.5 mJ/cm^2 radiation exposure at the surface of the sample.

All the phantoms for this study were based on water solutions of 2% agar (GMB, Russia) to model the acoustical impedance of biological soft tissues [17]. For use with our Specord 250 plus (Analytik Jena, Germany) spectrophotometer, water solutions of lipofundin (B.Braun, Germany) and black drawing ink (Kokh-i-Nor, Czech Republic) were prepared to mimic [18] the possible optical properties of different biological tissues at the 532 nm wavelength. The reduced optical scattering coefficients of the 0.5% and 10% lipofundin solutions were estimated as 6 and 120 cm^{-1}, respectively, (the higher value is typical of skin and the lower value is typical of other biological soft tissues [2]).

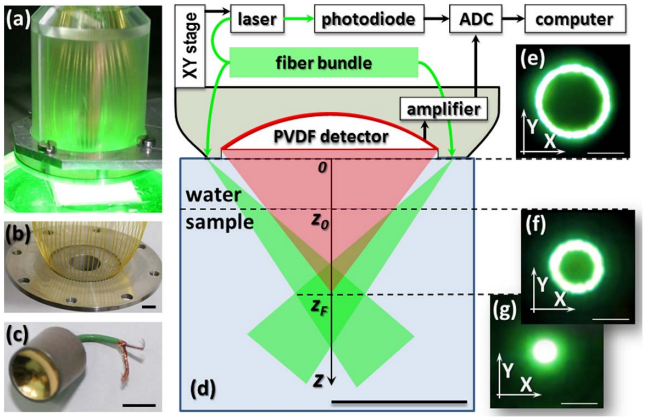

Fig. 1. Experimental setup for OA/US/DR imaging, all bars are 5 mm. (a) Photograph of the scanning OA head; (b) ferrule containing the outputs of 70 fibers for optical illumination of the object with the hole for the PVDF detector; (c) spherically focused PVDF optoacoustic detector; (d) schematic of the experimental setup and the axial geometry of the optoacoustic focus; (e)–(g) lateral geometry of optical illumination, measured at different depths in water.

The optical absorption of 4% of the black ink was estimated as 220 cm^{-1}, which is typical of blood [2] near the 531 nm isosbestic point of oxygenated and deoxygenated hemoglobin.

Each laser pulse triggers a 16 bit two-channel CSE1622 (Gage, USA) analog-to-digital converter (ADC) to collect the beam-sampling signal from a det10a photodiode (Thorlabs, USA) and the PVDF detector. The photodiode contains a custom-made built-in integration circuit expanding the effective pulse duration to ~50 ns for better compatibility with the 200 MS/s acquisition rate of the ADC. The PVDF detector has a custom-made 30 dB amplifier with a 3 MHz high-pass filter. The high-pass filter is required to avoid unnecessary correlation of the OA and US signals with the low-frequency pyroelectric signal generated due to heating of the PVDF film by the reflected photons.

An algorithm automatically acquires the envelopes of the time-spaced DR/OA/US signals (Fig. 2) using Hilbert's transform. As the diffuse photons back-scatter toward the surface of the PVDF detector, the DR signal is first acquired [Fig. 2(a)], allowing estimation of the diffuse reflectance from the sample at any given XY position of the scanning head. Due to the pyroelectric effect, the relaxation of the DR signal to zero takes ~200 ns, which, however, does not limit the acquisition window of the OA and US modalities.

The measured amplitude of the DR signal can also be interpreted as the amplitude of the probing laser-ultrasound pulse [12] propagating from the spherical surface of the PVDF detector into the sample. For example, at the time $t_{OA} = F/c$ when the US probing pulse reflects from the copper wire, providing both the OA and US contrast, the OA signal from the same wire is being detected [Fig. 2(b)]. Then, the echo US signal [Fig. 2(c)] travels to the PVDF detector and is registered at time $t_{US} = 2F/c$. The delay in propagation of the US pulses in respect of the OA ones doubles the effective spatial sampling for the US modality [Fig. 2(c)]. Assuming $c = 1.52$ mm/μs is the speed of sound in the sample, the 200 MS/s sampling rate of the ADC gives $\Delta z_{OA} = 7.6$ μm and $\Delta z_{US} = 3.8$ μm as the spatial sampling interval estimates for the OA and US modalities, respectively. Since the geometry [Fig. 1(d)] of the triple-modality system we have developed satisfies the condition $(z_F - z_0) < F/2$, the temporal separation of the OA and US signals does not limit the diagnostic depths of the OA and US modalities.

Sub-nanometer differences in optical skin depths [19] and micrometer differences in thermal skin depths [20] for copper and gold cannot be distinguished by a 35 MHz optoacoustic detector. Different durations of DR/OA/US signals of 20/36/51 ns, respectively, are due to the frequency-dependent US attenuation [21]. With 1 dB/cm/MHz acoustic absorption the acoustic path for the US probing pulse $2F = 1.4$ cm will at-

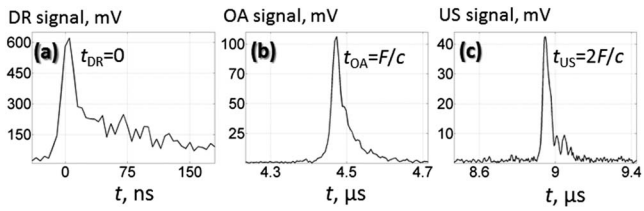

Fig. 2. Typical temporal DR/OA/US signals acquired from the OA A-scan of the phantom. (a) DR signal from the light-scattering background made of the water solution of 2% agar and 0.5% lipofundin; (b) OA A-line signal from the 50 μm copper wire located at the focus; (c) US A-line signal from 50 μm copper wire located at the focus.

tenuate the signal at the 50 MHz frequency of the detector by 70 dB, while at the 20 MHz frequency of the detector the signal will be attenuated only by 28 dB.

The resolution of the DR/OA/US modalities was measured in phantom, based on a water solution of 2% agar and 0.5% lipofundin containing 10 μm of aluminum foil located at the depth of the OA focus [Fig. 3(a)]. The dots in Figs. 3(b) and 3(c) represent the OA and US axial profiles of the aluminum foil. The blue lines represent the Gaussian fit $A\ \exp[-(z-\zeta)^2/\sigma_z^2/2]$ to the OA and US axial data. *Full width at half-maximum* (FWHM) for the Gaussian distribution FWHM $\approx 2.36\sigma_z$ provides the estimated values of the axial resolution of the OA and US modalities as 38 and 26 μm, respectively. The major reason the US modality can demonstrate a better axial resolution is its doubled spatial sampling rate. US axial resolution is, however, more affected by frequency-dependent US attenuation in comparison to an OA one.

To estimate the lateral resolution of the DR/OA/US modalities, the edge of the aluminum foil was scanned along the X axis with a $\Delta x = 2$ μm step size. Figures 3(d)–3(f) represent the *maximum intensity projection* (MIP) of the DR/OA/US signals fitted by the integral of the Gaussian function $C - B\sqrt{2\pi}\sigma_x \mathrm{erf}[\sqrt{2}(\chi - x)/(2\sigma_x)]$. The lateral resolutions of the DR/OA/US modalities, estimated as FWHM $\approx 2.36\sigma_x$, are 3.5 mm/50 μm/35 μm, respectively. The lateral resolution of the US modality being $\sqrt{2}$ times greater than the OA one is caused by two factors. The first factor is the low scattering of the laser-ultrasound probing pulse for the US modality (in comparison with the optical pulse for the OA modality). Second, the US modality uses the same focusing surface both for emitting the probing US pulse and for receiving the US echo pulse, while the optical and US foci of the OA modality have different geometries.

Since the reflecting edge of the aluminum foil [Fig. 3(a)] was placed beyond the 1.7 mm transport length, the measured lateral spatial resolution of the DR modality [Fig. 3(d)] exceeded the ~3 mm effective lateral size of the optical focus measured in water [Fig. 1(g)]. Importantly, the spherical surface of the PVDF detector coated by a submicron layer of gold also contributes to the lateral XY resolution of the DR imaging. According to [22], optical illumination of the gold at the 532 nm wavelength provides for maximal 26% absorbance in the case of 0° incident angle, however, when the incidence angle increases from 30° to 90° the absorbance of the gold decreases and drops to zero. Therefore, the back-scattered photons emerging from the acoustic focus better contribute to the DR signal, than the out-of-focus ones.

Possible limitations of such triple-modality imaging are, however, connected with the dependability of the amplitudes of the DR/OA/US signals. For example, while the DR signal is limited by the ±5 V dynamic range of the ADC, the amplitude of the US signal from the 50 μm copper wire [Fig. 2(c)] is one order of magnitude lower than the DR signal [Fig. 2(a)]. Similarly, the diffuse reflectance from a highly scattering sample can significantly exceed the amplitude of the OA signal. Nevertheless, the problem of adaptation of the DR/OA/US dynamic ranges to samples with arbitrary optical and acoustical properties can be easily solved by the development of a three-channel amplifier with individually tunable gains on each channel. A commercially available nanosecond switcher such as the ADG711 (AnalogDevices, USA) can then be automated to sequentially plug the PVDF detector through the individual amplifiers for the different DR/OA/US modalities.

To demonstrate the potential of such simultaneous triple-modality DR/OA/US imaging, a phantom with inhomogeneous optical and acoustic properties was developed [Fig. 4(a)]. The phantom background was based on a water solution of 2% agar and 0.5% lipofundin. The left side of the phantom contained the heterogeneity of optical scattering provided by a 0.1 ml injection of 10% lipofundin. The right side of the phantom contained a 0.1 ml injection of a 4% water solution of black drawing ink. Seven copper wires of 50 μm diameter crossed the center of the phantom, with the deepest wire located at a depth of

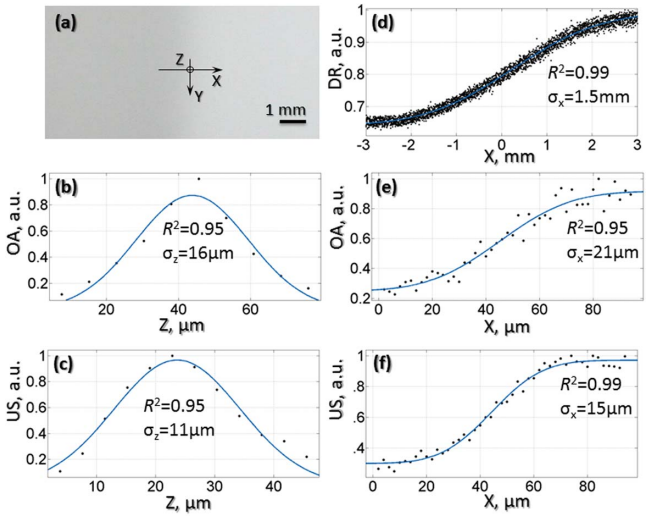

Fig. 3. Resolution of the DR/OA/US modalities. (a) photograph of the agar phantom with the edge of the aluminum foil oriented along the Y axis; (b), (c) the OA/US axial profiles of the 10 μm aluminum foil acquired from the same A-scan, and their Gaussian fits; (d)–(f) the DR/OA/US MIP signals profiling the edge of the aluminum foil in the lateral direction and their fits by the integral of the Gaussian function.

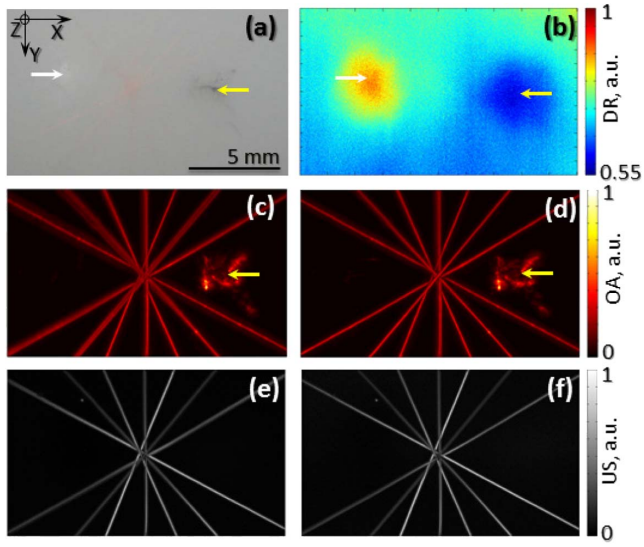

Fig. 4. Results of DR/OA/US imaging of the phantom. (a) photograph of the agar phantom containing seven copper wires, the injection of lipofundin is marked by the white arrow, and the injection of black ink is marked by a yellow arrow; (b) MIP DR image; (c), (d) MIP OA images before and after the reconstruction; (e), (f) MIP US images before and after reconstruction [23].

approximately 3 mm from its surface. To provide two-dimensional triple-modality DR/OA/US imaging, the phantom [Fig. 4(a)] was scanned in the XY directions with $\Delta x = \Delta y =$ 15 μm scanning steps.

Figure 4(b) represents the DR MIP image. The bright spot shows the position of the heterogeneity in the optical scattering, responsible for a greater number of back-scattered photons with respect to the number of them acquired at other XY positions of the scanning head. The black spot indicates the position of the heterogeneity of optical absorption that reduces the number of them back-scattered from the sample. Although the copper wires do provide optical contrast against the background, they cannot be distinguished in the DR image due their smaller size in respect to the resolution of the DR modality.

Figure 4(c) represents the MIP image of the OA signals. The heterogeneities of the optical absorption (the copper wires and the black ink injection) are clearly seen in the OA image while the heterogeneity of the optical scattering [Fig. 4(b)] does not provide OA contrast [Fig. 4(c)]. Since some of the wires are located out of the acoustic focus, the MIP OA image formed from the raw OA data [Fig. 4(c)] contains out-of-plane artifacts, are removed at Fig. 4(d) using a reconstruction algorithm [23].

Figures 4(e) and 4(d) represent the MIP US images of the phantom before and after reconstruction [23]. Since the water injections of lipofundin and black ink were not able to significantly modify the acoustic impedance of the homogeneous agar background, the copper wires provided the strongest US contrast and are clearly seen in these images.

Although the DR modality complements the OA one by imaging the heterogeneity of the optical scattering [Fig. 4(b)], there is yet another prospective reason to use DR/OA in combination. Local optoacoustic pressure measured by the PVDF detector is defined by the product of two unknown optical parameters, the fluence and the absorption. From a clinical point of view, the optical absorption coefficient is the more important parameter. Quantitatively measured at different laser wavelengths, the optical absorption coefficient provides valuable diagnostic information about the tissue chromophore concentrations with known optical spectra. Unfortunately, the unknown spatial distribution of the fluence limits the opportunities for multispectral quantitative OA measurements [24]. Nevertheless, since the diffuse reflectance is independently related to each of the fluence and the absorption [25], the DR signal can be used to simplify the inverse problems of quantitative OA imaging. Previous works that utilized diffuse optical methods to improve OA quantifications include the following [26–28].

Therefore, this Letter presents the idea of a cost-effective modification of an acoustic resolution photoacoustic microscope to provide triple-modality DR/OA/US imaging. Since the DR/US modalities of our system utilize the conventional OA hardware, the proposed principle of simultaneous DR/OA/US imaging could be used in many of the OA systems (including tomographic ones) of other authors [29–31]. This phantom study demonstrates the opportunities for new systems to provide simultaneous imaging of the various optical and acoustic heterogeneities that can be contained inside biological tissues. Future work is planned to undertake *in vivo* experiments.

Funding. Russian Science Foundation (RSF) (14-15-00709); Russian Foundation for Basic Research (RFBR) (13-02-01289, 14-02-00836).

Acknowledgment. The author is grateful to the Russian Science Foundation for the equipment and to the Russian Foundation for Basic Research for other forms of support during the development of the experimental setup. The author is grateful to Maxim Prudnikov, Vladimir Vorobiev, and Roman Belyaev for their technical contributions to this work; to Andrey Kovalchuk, and Dr. Ilya Fiks for their help with the automation of this new system; to Dr. Michael Jaeger for his provision of the reconstruction algorithm; and to Dr. Ilya Turchin for his valuable discussions.

REFERENCES

1. P. Beard, Interface Focus **1**, 602 (2011).
2. S. L. Jacques, Phys. Med. Biol. **58**, R37 (2013).
3. V. Ntziachristos, Nature Methods **7**, 603 (2010).
4. L. V. Wang and S. Hu, Science **335**, 1458 (2012).
5. A. Taruttis and V. Ntziachristos, Nat. Photonics **9**, 219 (2015).
6. M. Omar, D. Soliman, J. Gateau, and V. Ntziachristos, Opt. Lett. **39**, 3911 (2014).
7. H. F. Zhang, K. Maslov, G. Stoica, and L. V. Wang, Nat. Biotechnol. **24**, 848 (2006).
8. C. Xu, P. D. Kumavor, A. Aguirre, and Q. Zhu, J. Biomed. Opt. **17**, 0612131 (2012).
9. M. Jaeger, K. Gashi, H. G. Akarçay, G. Held, S. Peeters, T. Petrosyan, S. Preisser, M. Gruenig, and M. Frenz, Photon. Lasers Med. **3**, 343 (2014).
10. R. Bouchard, O. Sahin, and S. Emelianov, IEEE Trans. Ultrason. Ferroelectr. Freq. Control **61**, 450 (2014).
11. F. Gao, X. Feng, and Y. Zheng, Appl. Phys. Lett. **104**, 213701 (2014).
12. G. Wurzinger, R. Nuster, N. Schmitner, S. Gratt, D. Meyer, and G. Paltauf, Biomed. Opt. Express **4**, 1380 (2013).
13. J. Xia, C. Huang, K. Maslov, M. A. Anastasio, and L. V. Wang, Opt. Lett. **38**, 3140 (2013).
14. M. Jaeger, D. Harris-Birtill, A. Gertsch, E. O'Flynn, and J. Bamber, J. Biomed. Opt. **17**, 066007 (2012).
15. P. Subochev, A. Katichev, A. Morozov, A. Orlova, V. Kamensky, and I. Turchin, Opt. Lett. **37**, 4606 (2012).
16. P. Subochev, I. Fiks, M. Frenz, and I. Turchin, Laser Phys. Lett. **13**, 025605 (2016).
17. K. Zell, J. Sperl, M. Vogel, R. Niessner, and C. Haisch, Phys. Med. Biol. **52**, N475 (2007).
18. P. Di Ninni, Y. Bérubé-Lauzière, L. Mercatelli, E. Sani, and F. Martelli, Appl. Opt. **51**, 7176 (2012).
19. G. Diebold, T. Sun, and M. Khan, Phys. Rev. Lett. **67**, 3384 (1991).
20. Y. Hou, S. Ashkenazi, S.-W. Huang, and M. O'Donnell, IEEE Trans. Ultrason. Ferroelectr. Freq. Control **54**, 682 (2007).
21. V. P. Zharov and V. S. Letokhov, *Laser Optoacoustic Spectroscopy* (Springer, 2013), Vol. **37**.
22. D. Bergström, J. Powell, and A. Kaplan, J. Appl. Phys. **101**, 113504 (2007).
23. M. Jaeger, S. Schüpbach, A. Gertsch, M. Kitz, and M. Frenz, Inverse Prob. **23**, S51 (2007).
24. B. Cox, J. G. Laufer, S. R. Arridge, and P. C. Beard, J. Biomedical Optics **17**, 0612021 (2012).
25. S. L. Jacques, J. Biomed. Opt. **15**, 051608 (2010).
26. C. Xu, P. D. Kumavor, U. Alqasemi, H. Li, Y. Xu, S. Zanganeh, and Q. Zhu, J. Biomed. Opt. **18**, 126006 (2013).
27. L. Xi, X. Li, L. Yao, S. Grobmyer, and H. Jiang, Med. Phys. **39**, 2584 (2012).
28. A. Q. Bauer, R. E. Nothdurft, T. N. Erpelding, L. V. Wang, and J. P. Culver, J. Biomed. Opt. **16**, 096016 (2011).
29. B. Ning, M. J. Kennedy, A. J. Dixon, N. Sun, R. Cao, B. T. Soetikno, R. Chen, Q. Zhou, K. Kirk Shung, and J. A. Hossack, Opt. Lett. **40**, 910 (2015).
30. A. Mandelis, X. Guo, B. Lashkari, S. Kellnberger, and V. Ntziachristos, "Wavelength-modulated differential photoacoustic spectroscopy (WM-DPAS) for noninvasive early cancer detection and tissue hypoxia monitoring," J. Biophoton., doi: 10.1002/jbio.201500131.
31. C.-W. Wei, T.-M. Nguyen, J. Xia, B. Arnal, E. Y. Wong, I. M. Pelivanov, and M. O'Donnell, IEEE Trans. Ultrason. Ferroelect. Freq. Control **62**, 319 (2015).